



Selection of radio pulsar candidates using artificial neural networks

R. P. Eatough,^{1,2}★ N. Molkenthin,¹ M. Kramer,^{1,2} A. Noutsos,¹ M. J. Keith,^{1,3}
B. W. Stappers¹ and A. G. Lyne¹

¹Jodrell Bank Centre for Astrophysics, Alan Turing Building, School of Physics and Astronomy, The University of Manchester, Manchester M13 9PL

²Max-Planck-Institut für Radioastronomie, Auf dem Hügel 69, 53121 Bonn, Germany

³Australia Telescope National Facility, CSIRO, PO Box 76, Epping, NSW 1710, Australia

Accepted 2010 May 22. Received 2010 May 8; in original form 2010 March 25

ABSTRACT

Radio pulsar surveys are producing many more pulsar candidates than can be inspected by human experts in a practical length of time. Here we present a technique to automatically identify credible pulsar candidates from pulsar surveys using an artificial neural network. The technique has been applied to candidates from a recent re-analysis of the Parkes multi-beam pulsar survey resulting in the discovery of a previously unidentified pulsar.

Key words: methods: data analysis – stars: neutron – pulsars: general.

1 INTRODUCTION

Since the discovery of pulsars by Jocelyn Bell and Antony Hewish at Cambridge in 1967 using a pen chart recorder (Hewish et al. 1968), pulsar searching has come a long way. Modern pulsar surveys use high performance computing facilities to perform an extensive range of signal processing and search algorithms. These methods are designed to maximize sensitivity to weak, rapid and dispersed pulsar signals often buried in large amounts of terrestrial radio frequency interference (RFI) or even in binary systems. There is little doubt that these complex algorithms have aided searches for pulsars; however, there remain certain search tasks for which standard computer programs are of little use. In particular, the final stage of a pulsar search, the selection of credible pulsar candidates for follow-up observations, still remains a task for a human since the decision is visual and based on a number of combined properties of the pulsar signal. The process can be time consuming and inefficient in analysis of large-scale surveys that produce many millions of pulsar candidates.

Large-scale pulsar surveys, such as the Parkes multi-beam pulsar survey (PMPS; Manchester et al. 2001), have dramatically increased the number of known pulsars. Finding more pulsars elucidates the properties of their Galactic population and also offers the possibility of uncovering new and extreme phenomena in neutron-star astrophysics. Future pulsar surveys will be done with the next generation of radio telescopes, such as LOw Frequency ARray (LOFAR; van Leeuwen & Stappers 2010), the Five hundred metre Aperture Spherical Telescope (FAST; Smits et al. 2009b) and the Square Kilometre Array (SKA; e.g. Cordes et al. 2004; Smits et al. 2009a). These radio telescopes will be excellent survey tools because of their large collecting areas, capability to form many simultaneous beams on the sky and, in the case of the interferometers, wide fields

of view. It is expected that these instruments will detect a large fraction of the observable pulsars in the Galaxy. The inevitable flood of pulsar candidates that will require inspection to achieve this will certainly require some form of multiperson or machine-based candidate selection. Some large-scale astronomical surveys and data mining projects have resorted to employing many online volunteers to search for or classify their objects of interest in so-called citizen science projects (e.g. Westphal et al. 2005; Lintott et al. 2008). In searches for pulsars, the pulsar Arecibo L-band Feed Array (ALFA) survey collaboration has enlisted the help of high school and undergraduate students in a successful outreach and science programme to identify potential pulsar candidates (Jenet et al. 2007).

Recent machine solutions include candidate ranking based on likelihoods calculated from parameter distributions of pulsar and non-pulsar signals (Lee, private communication) and the sorting of candidates based on a number of ‘scores’ that indicate the similarity of the signal to that of a typical pulsar (Keith et al. 2009). In this paper, we present an alternative method whereby an artificial neural network (ANN) has been trained using a particular set of scores to automatically identify credible pulsar candidates from a recent re-analysis of the PMPS. ANNs have long been used in other areas of astronomy, for example in the morphological classification of galaxies (e.g. Storrie-Lombardi et al. 1992; Zhang, Li & Zhao 2009), in the estimation of photometric redshifts of sources in the Sloan Digital Sky Survey (Firth, Lahav & Somerville 2003) and in the selection of microlensing events from large variability surveys (Belokurov, Evans & Du 2003).

The outline of this paper is as follows. In Section 2, we describe how pulsar candidate selection in our recent re-analysis of the PMPS is typically done and some of the problems associated with this method. Section 3 gives a brief introduction to ANNs. In Section 4, we describe our implementation of an ANN to classify pulsar candidates from our re-analysis of the PMPS and the results from a test on a sample of the search output data. Preliminary parameters of the pulsar discovered using an ANN during our

★E-mail: reatough@mpifr-bonn.mpg.de

re-analysis of the PMPS are given in Section 5. Finally, Section 6 gives a summary, followed by a discussion of the future application of ANNs to pulsar surveys.

2 CANDIDATE SELECTION

The process of searching for undiscovered pulsars can be separated into two distinct stages: first, the survey data are acquired at radio telescopes and then processed using the standard search methods; secondly, the output of the processing is analysed to select good pulsar candidates for follow-up observation. Detailed descriptions of the steps involved in the first stage of a pulsar search can be found in, for example, Lorimer & Kramer (2005). The second stage, which is the subject of this paper, is typically done by visual inspection of the pulsar candidates generated from the initial processing. Using a graphical selection tool, such as REAPER (Faulkner et al. 2004) or more recently JREAPER (Keith et al. 2009), each pulsar candidate can be presented as a point on a two-dimensional phase-space diagram like those displayed in Figs 1(a) and (b). In this example, candidates from 650 survey beams of our latest re-analysis of the PMPS with acceleration searches (Eatough 2009, Eatough et al., in preparation) are plotted on axes of barycentric pulse period versus signal-to-noise ratio (S/N). Large numbers of spurious candidates

due to RFI are visible as ‘columns’ in this phase space. Selecting a point in the phase diagram would reveal the so-called candidate plot for the pulsar candidate in question. Each candidate plot contains a number of associated diagnostic plots designed to help assess the credibility of pulsar candidates. Examples of two such candidate plots can be seen in Figs 2(a) and (b). Fig. 2(a) shows the candidate plot of PSR J1926+0739, discovered in this work using an ANN (see Section 5). Fig. 2(b) shows one of the many spurious pulsar candidates that is most likely the result of terrestrial RFI. To a pulsar astronomer searching this phase space, or indeed any individual with modest training, a distinction between genuine or credible pulsar candidates and those due to RFI or random statistical fluctuations can easily be made, making it possible to pick out good pulsar candidates that should be marked for follow-up observation. Common features of genuine pulsar candidates include a narrow pulse width, typically around 5 per cent of the pulse period; a pulse present over all the sub-integrations; pulse phase coherent emission across all frequency sub-bands; an ‘island’ in the period–dispersion measure (DM) diagram; good agreement between the real and theoretical DM–S/N curves; and good agreement between the real and theoretical acceleration–S/N curves. Millisecond and binary pulsars often exhibit slight differences to normal pulsars in their candidate plots. Again, these differences are easily recognizable by a human expert. It should be noted that exceptions to the above characteristics do occur and in general each pulsar displays a unique signature in its candidate plot.

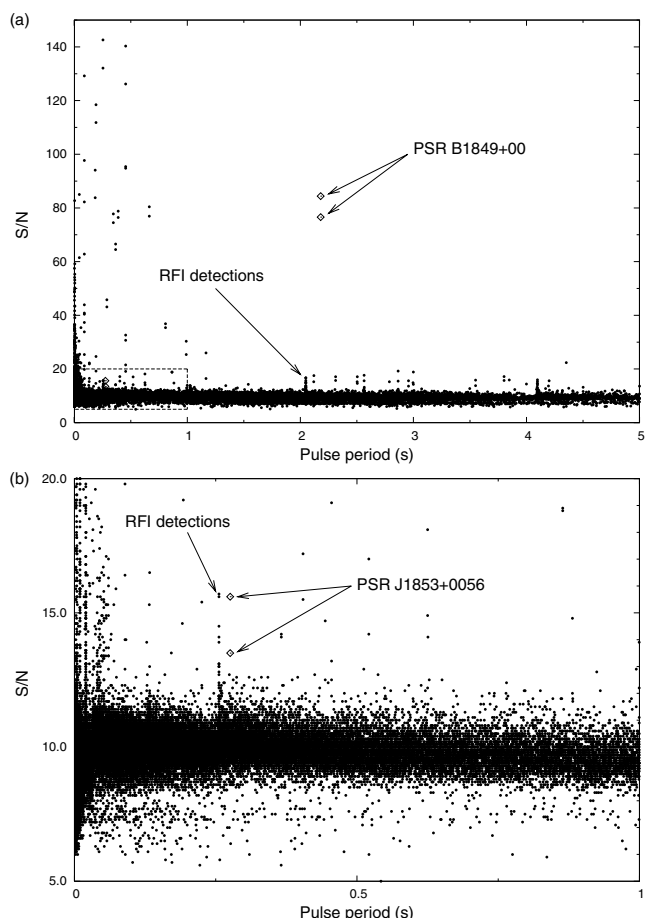


Figure 1. The barycentric pulse period–S/N distribution of candidates from 650 survey beams of the PMPS. Panel (a) shows the entire sample with two detections of PSR B1849+00 highlighted. The area enclosed by the box in the bottom left is shown in panel (b). Here the positions of two detections of PSR J1853+0056 have been marked.

2.1 The candidate selection problem

Although graphical tools have reduced the number of candidate plots that need to be inspected, by allowing RFI signals to be easily avoided, there are still many more than can be effectively viewed by a human in a reasonable length of time. This is especially true if the more numerous, weaker candidates (where the majority of undiscovered pulsars will be found) are probed. Typically, our search algorithms produce around 200 candidate pulsar plots per survey beam. In the PMPS, $\sim 40\,000$ survey beams were performed. Using our current search algorithms, this gives a total of ~ 8 million pulsar candidates for visual inspection. In our search for fast binary pulsars, the PMPS beams have been split into two independent halves effectively doubling this number. The typical time taken to inspect a candidate pulsar depending on its credibility can lie between 1 and ~ 300 s. As an example, a data base of 1 million candidate pulsars would take somewhere between 12 d and 10 yr of continuous viewing to search. In our search for highly accelerated pulsars, the inspection time is often over an hour as different acceleration algorithms and integration lengths are used to find the optimal detection S/N. Because viewing the pulsar candidates takes large amounts of time, fatigue can also increase the potential for human error.

We wish to increase the speed and efficiency with which pulsar candidates can be searched and also to avoid the arbitrary ‘cuts’ that graphical selection tools impose, such as ignoring all candidates near RFI signals and those in the noise floor. One solution has been to rank pulsar candidates not simply by their S/N but based on a number of scores from the diagnostic plots that indicate the similarity of the signal to that of a typical pulsar (Keith et al. 2009). This method has had a remarkable amount of success, particularly at finding weaker pulsars that were missed in previous analysis of the PMPS. However, the decision boundary on the credibility of a pulsar candidate is complex and is based on the combined features of each of the diagnostic plots and how they relate to each other for the particular candidate in question. A simple example of such

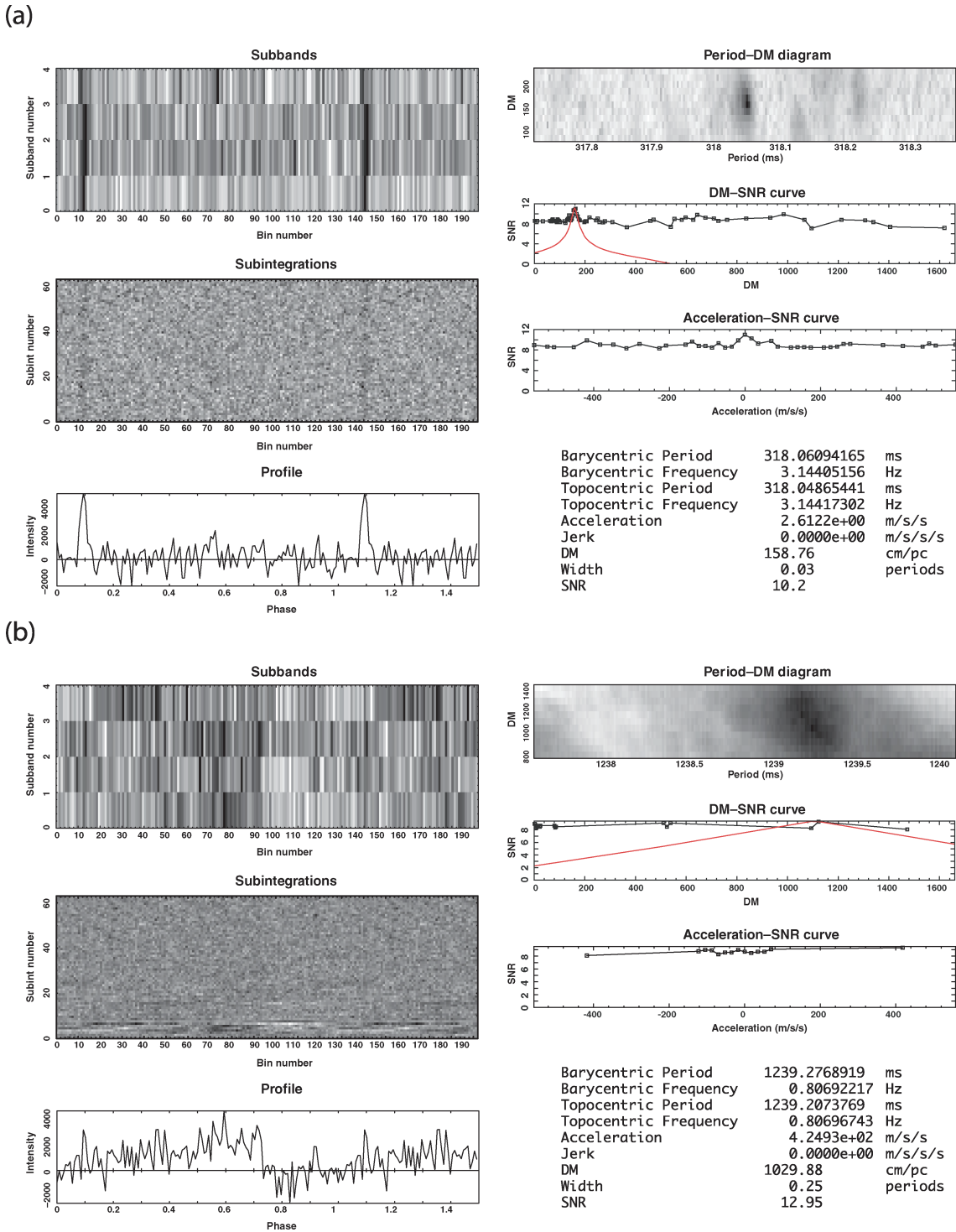


Figure 2. Example pulsar candidate plots. Panel (a) shows PSR J1926+0739, discovered in this work using an ANN (see Section 5). Panel (b) shows a typical pulsar candidate that is most likely the result of RFI. Starting clockwise from the bottom left, the two candidate plots display the integrated pulse profile, folded at the optimum period and DM; 64 temporal sub-integrations of the observation, showing how the pulse varies with time; stacked pulses across four frequency sub-bands, showing how the pulse varies with observing frequency; the period-DM diagram, which shows how the S/N varies with small changes in the folding period and DM; the spectral S/N as a function of a wide range of trial DMs (the DM-S/N curve); and finally the spectral S/N as a function of trial acceleration (the acceleration-S/N curve).

a relation is that longer period pulsars, or those with larger pulse widths, exhibit somewhat flatter DM–S/N curves. In practice, there are many more relations between the features displayed in each of the diagnostic plots. At the moment, scoring algorithms cannot

account for these relations and only provide features to weight the individual scores.

Here we present an extension to the scoring method whereby an ANN has been trained, using a set of scores, to attempt to model

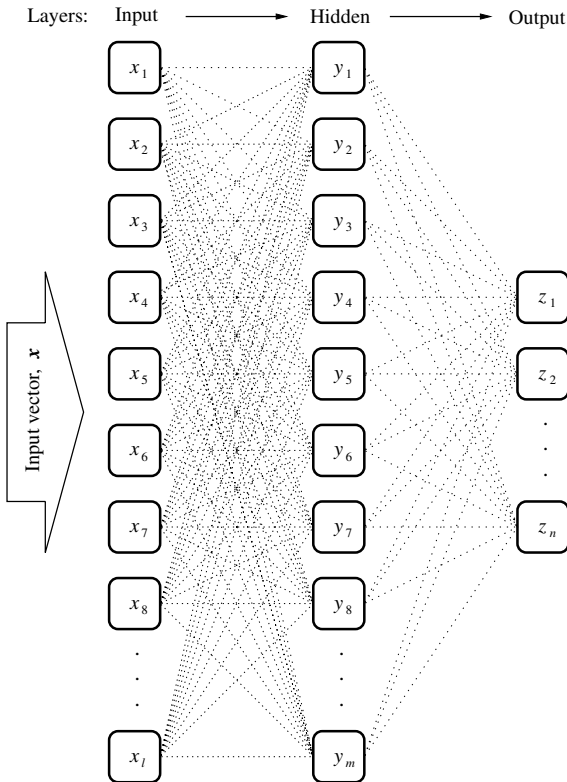


Figure 3. A schematic diagram of a general three-layered ANN of the type used in this work.

these complex decisions and automatically identify credible pulsar candidates. First, we give a brief introduction to ANNs.

3 ARTIFICIAL NEURAL NETWORKS

An ANN is a computational technique based loosely upon models of the behaviour of the human central nervous system. They have applications to problems where some form of non-parametric estimation is required, i.e. where no known theory can be used to model the properties of a set of data. Examples might include speech or pattern recognition. For a more detailed description of ANNs and their applications, see for example Bishop (1995). A simplified picture based on ANNs used in this work is as follows.

A number of nodes¹ are arranged into layers usually comprising an input layer, any number of hidden layers and an output layer. The architecture of an ANN can be written simply by indicating the number of nodes in each of these layers. For example, one of the ANNs used in this work has 12 nodes in the input layer, 12 nodes in one hidden layer and two nodes in the output layer giving the architecture 12:12:2. For simplicity, we now consider an architecture of just three layers with any number of nodes, as depicted in Fig. 3. The input layer takes the ‘input vector’, $\mathbf{x} = x_1, x_2, x_3, \dots, x_l$, a set of parameters to be passed to the ANN. The hidden layer can also be written as a vector, $\mathbf{y} = y_1, y_2, y_3, \dots, y_m$, and the output layer by another, $\mathbf{z} = z_1, z_2, z_3, \dots, z_n$. The nodes in each layer are connected to all the nodes in the previous layers. At each node in the hidden layer y_j , a linear-weighted sum S_j^y of the

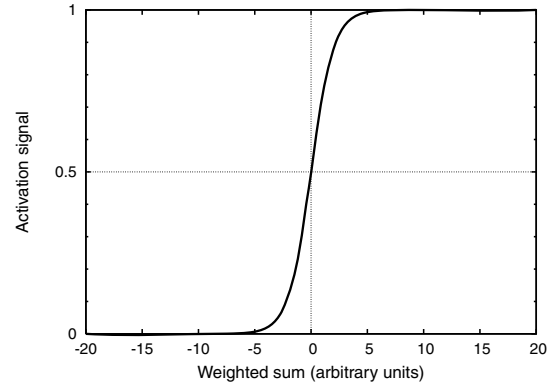


Figure 4. An example sigmoid activation function. Using this function, the output of each node can be interpreted as a posterior probability.

values from the previous layer is calculated:

$$S_j^y = \sum_{i=1}^l w_{ij} x_i, \quad (1)$$

where $i = 1, 2, 3, \dots, l$ in the x layer, $j = 1, 2, 3, \dots, m$ in the y layer and w_{ij} are weights associated between nodes in each layer and which initially take random values. Positive weights represent ‘affirmative’ connections and negative weights represent ‘inhibitory’ connections. The so-called activation function, usually of a sigmoid form, is calculated in the interval from 0 to 1 (to control the amplitude of the output of a node whatever the magnitude of the weighted sum; see Fig. 4) and assigned to each element in the y layer:

$$y_j(S_j^y) = 1/[1 + \exp(-S_j^y)]. \quad (2)$$

These values are then passed to the next layer (in our case the output layer, z) where another set of weighted sums, $S_k^z = \sum_{j=1}^m w_{kj} y_j$, is used to compute the next set of activation functions, $z_k(S_k^z)$ for $k = 1, 2, 3, \dots, n$. Because this is the last layer, the values of these functions constitute the output values of the ANN.

In a process of so-called supervised learning, the ANN is trained by comparison of the values from the output layer, z , with a desired output vector, \mathbf{d} , that is pre-determined by a human. The comparison is usually done via the evaluation of a cost function often called the ‘error’, E . In ‘batch supervised learning’ the error function is averaged over many input vectors, i.e. a training set, in one training iteration, t . Training is executed by a process of modifying the weights in the next training cycle, $(t+1)$, to minimize the error function, E . This is done in reverse starting at the output layer and ending up at the input layer, in the so-called backpropagation phase:

$$w_{ij}(t+1) = w_{ij}(t) + \Delta w_{ij}(t+1), \quad (3)$$

where $\Delta w_{ij}(t+1)$ are the sum of the weight modifications between the input layer and the hidden layer in the $(t+1)$ th cycle. Exactly how the weights are modified, i.e. the value of $\Delta w_{ij}(t+1)$, depends upon the learning model chosen. In our system, we have chosen Resilient backPROPaGation (RPROP), where the size of $\Delta w_{ij}(t+1)$ is fixed and depends only upon the sign of a partial derivative, $\partial E / \partial w_{ij}$. For a detailed description of the RPROP learning function, see the Stuttgart Neural Network Simulator (SNNS) user manual, version 4.2 and references therein.² The RPROP error function to be minimized

¹ Here, the term ‘nodes’ represents individual processing elements of a computer program.

² <http://www.ra.cs.uni-tuebingen.de/SNNS/>

is given by

$$E = \sum (z_k - d_k)^2 + 10^{-\alpha} \sum w_{ij}^2, \quad (4)$$

where α is an additional free parameter called the ‘weight-decay’ term. Once training is complete, the weights are fixed and the ANN can be fed input vectors with no training parameters. Any of these vectors similar to those in the training set should produce output vectors similar to the initial desired vector d .

4 IMPLEMENTATION IN RE-ANALYSIS OF THE PMPS

The decision was taken to analyse some of the ~ 16 million pulsar candidates generated by our re-analysis of the PMPS using an ANN. All ANNs presented in this work have been implemented using SNNS.

4.1 Candidate scores

As input to the ANNs, small but characteristic input vectors were formed from various candidate parameters and each of the panels displayed in the candidate plots was generated by our search software (Figs 2a and b). Each element of the input vector, which we term score, was designed to draw a distinction between pulsar-like and non-pulsar-like signals, caused by RFI or random statistical fluctuations (noise). In total 12 scores, listed in Table 1, were used. Scores nine to 12 were introduced to better represent the two-dimensional sub-band and sub-integration panels in the candidate plots. More details on the features of candidate plots and scoring pulsar candidates can be found in Keith et al. (2009). Pre-processing of the candidate plots in this way is beneficial both computationally and because of the so-called curse of dimensionality, which requires that the larger the number of input parameters the bigger the training set required to train the ANN effectively (see e.g. Bishop 1995, section 1.4). This prevents the use of the raw data that make up the candidate plot, for example the pulse profile, as an input. With these simple scores, pre-processing of the candidates for the ANN took a small fraction of the total data processing time.

Table 1. Summary of the scores used in the input vectors in this work. The ‘optimized’ curves refer to smaller finer searches in DM and acceleration around the initial detection values from the wider searches. Scores marked with a \clubsuit are additions only included in the 12:12:2 ANN.

No.	Score description
1	Pulse profile S/N
2	Pulse profile width
3	Chi-square of fit to theoretical DM–S/N curve
4	Number of DM trials with $S/N > 10$
5	Chi-square of fit to the optimized theoretical DM–S/N curve
6	Chi-square of fit to the theoretical acceleration–S/N curve
7	Number of acceleration trials with $S/N > 10$
8	Chi-square of fit to the optimized theoretical acceleration–S/N curve
9	rms scatter in sub-band maxima \clubsuit
10	Linear correlation across sub-bands \clubsuit
11	rms scatter in sub-integration maxima \clubsuit
12	Linear correlation across sub-integrations \clubsuit

A practical consideration worth mentioning at the pre-processing stage is that candidate files should be in a format that can be readily converted into input vectors for an ANN.

4.2 ANN architectures

Because of the large volume of data involved, only two ANN architectures have been investigated in this work. First, an 8:8:2 followed by a 12:12:2 ANN. In general, a large number of input parameters are beneficial since the input data can be better represented (up until the dimensionality problem takes effect). In addition ANNs with increased complexity have more free parameters, in the form of adjustable weights, and can in principle recreate more complicated decisions. However, increased complexity comes at the cost of computational efficiency. Large ANNs take longer to train and longer to process input data. A good balance between these factors is critical. In both ANNs investigated in this work each input vector has an equivalent number of elements in a hidden layer followed by an output layer comprising two elements, representing probabilities of the candidate being either a genuine pulsar or not a pulsar.

4.3 Training

To form our training set, 259 input vectors from a wide variety of known pulsars were used in addition to the vectors generated from 1625 non-pulsar signals due to RFI or noise fluctuations. As mentioned in Section 4.2 the output vector comprised of two elements, a genuine pulsar identification probability between 0 and 1 and a non-pulsar identification probability also between 0 and 1. During training, these outputs are pre-determined and form the desired output vector d . For real pulsars, $d = 1, 0$ and for RFI or noise signals, $d = 0, 1$. In accordance with ANN training procedures, a validation set of 28 different pulsars and 899 different RFI and noise signals were used. The development of the error, E , of our training and validation set with the training cycle for one of our ANNs can be seen in Fig. 5. One training cycle constitutes the sum over all the vectors in the training sample. Validation errors were also computed after every training cycle. All weights are initially set to random values. Optimum ANN training is achieved just before the error in the validation set begins to increase (SNNS user manual, version 4.2), in this case just before ~ 120 cycles. If training is continued after this point, the ANN is said to be ‘overtrained’ and

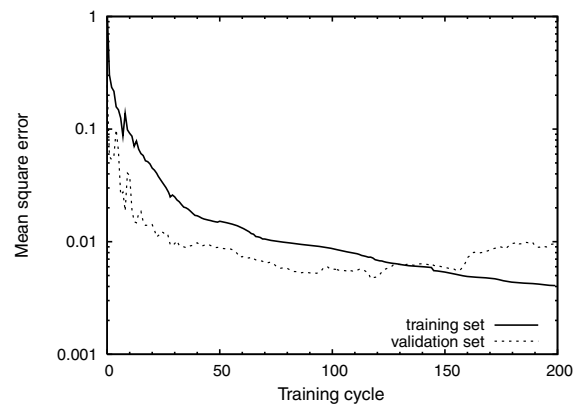


Figure 5. The error development of the training and validation sets in one of the ANNs investigated in this work. Training should be stopped around the cycle corresponding to the minimum in the validation set.

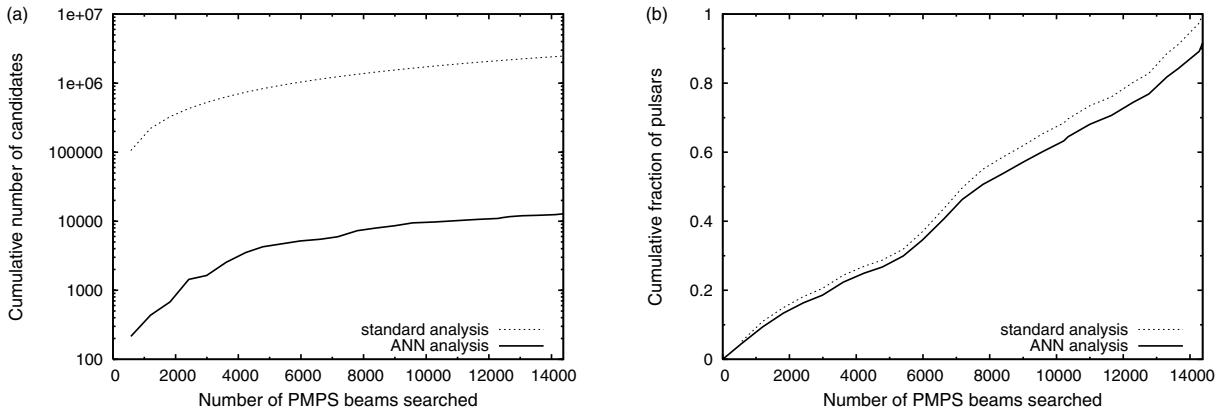


Figure 6. Panel (a) shows the cumulative number of candidates recovered by the standard analysis and the ANN over the results from $\sim 14\,400$ survey beams of our re-analysis of the PMPS. Panel (b) shows the cumulative fraction of known pulsars in the sample recovered by each method.

will not perform well on input vectors that do not match those in the training set precisely.

4.4 Test results

The 8:8:2 ANN has been tested on search results from a random selection of $\sim 14\,400$ survey beams from our re-analysis of the PMPS. Fig. 6 summarizes the results of both the standard graphical analysis and the analysis using the ANN. In Fig. 6(a), the cumulative number of candidates that would need inspection in a standard analysis, using a graphical selection tool, and in an analysis using an ANN is plotted against the number of PMPS beams searched. Fig. 6(b) displays the cumulative fraction of pulsars detected by each method. Our standard analysis shows that there are 501 detections of known pulsars in ~ 2.5 million pulsar candidates from the $\sim 14\,400$ beams. Due to constraints on the available amount of processed data, 51 of the 501 pulsars in the test sample were also present in the training set. Ideally, the test sample should be entirely independent of the training set to test if the ANN has been overtrained. In the ANN analysis, a candidate was flagged for viewing if the output vector of the ANN, $z = z_1, z_2$, had values $z_1 > 0.5$ and $z_2 < 0.5$, otherwise it was ignored. The number of candidates that filled this criterion was low, of the order of 0.5 per cent corresponding to around 13 000 candidates. Encouragingly, from the $\sim 13\,000$ candidates selected by the ANN 92 per cent of the pulsars present in the test sample have been recovered. This gives the statistics that one in every ~ 30 candidates selected by the ANN is a pulsar, whereas only one in every ~ 4900 candidates that would be viewed in a standard graphical analysis will be a real pulsar detection. Practical use of graphical selection tools means that not all the candidates would need to be viewed; however, this increases the risk of missing weak pulsars or those with similar periods to RFI signals. Ignoring the training pulsars that were present in the test sample reduces the recovered fraction of pulsars by 1 per cent.

The addition of four more scores in the 12:12:2 ANN marginally improved the recovered fraction of pulsars to 93 per cent. However the recovered number of candidates, along with the computation time, nearly doubled. This small improvement was somewhat expected. The relatively low resolution of the two-dimensional diagnostic plots in our re-analysis of the PMPS makes spotting statistical trends in these planes difficult. In the candidate plots from current and future pulsar surveys, these planes will be better sampled due to the increase in available computational power.

The properties of the pulsars missed by the ANN have been investigated. Distributions of spin period, pulse profile S/N, pulse duty cycle and DM for pulsars in the sample and those missed by the ANN are displayed in Fig. 7. There is no significant correlation between those pulsars missed and any property investigated. Two features of the distributions of missed pulsars are, however, worth noting. First, around 50 per cent of the pulsars with periods less than 10 ms were missed by the ANN. This result was somewhat expected and can be explained by the different appearance of the candidate plots associated with millisecond pulsars (MSPs). For example, MSPs can appear to have larger pulse widths because of the decreased number of phase bins across the pulse profile. Also, they exhibit narrow DM–S/N curves due to the rapid drop-off in sensitivity with incorrect DM trial. Unfortunately, only six MSP detections were present in the test sample making this result ambiguous. Secondly, 60 per cent of the pulsars with the profile S/Ns $\gtrsim 400$ are missing. This has been shown to be due to abnormal DM–S/N curves produced by our search software for extremely bright pulsars. The training set somewhat over-represented candidates from RFI or noise signals. This was done with the aim of identifying these more numerous candidates effectively; however, it could also have increased the number of false positives for this particular class. As a result, the other missing pulsars may simply have been misidentified.

The analysis of the ~ 2.5 million pulsar candidates using the 8:8:2 ANN took a total of ~ 50 CPU hours. Since the process is fully ‘parallelizable’ the task was easily distributed across a computer cluster.

5 DISCOVERY OF A PULSAR USING AN ANN

The ANN has been applied to a portion of candidates generated from our re-analysis of the PMPS with acceleration searches. In total, 14 pulsars have been discovered using standard candidate selection techniques (Eatough, Keane & Lyne 2009; Eatough *et al.* in preparation), and one has been found using the 8:8:2 ANN (see Fig. 2a). The pulsar, of provisional name PSR J1926+0739, has a spin period of ~ 318 ms, a DM of $\sim 160 \text{ cm}^{-3} \text{ pc}$ and was detected with an S/N of ~ 10 . This pulsar has been timed at the Jodrell Bank Observatory and is presented in Eatough (2009) with full astrometric and spin-down parameters.

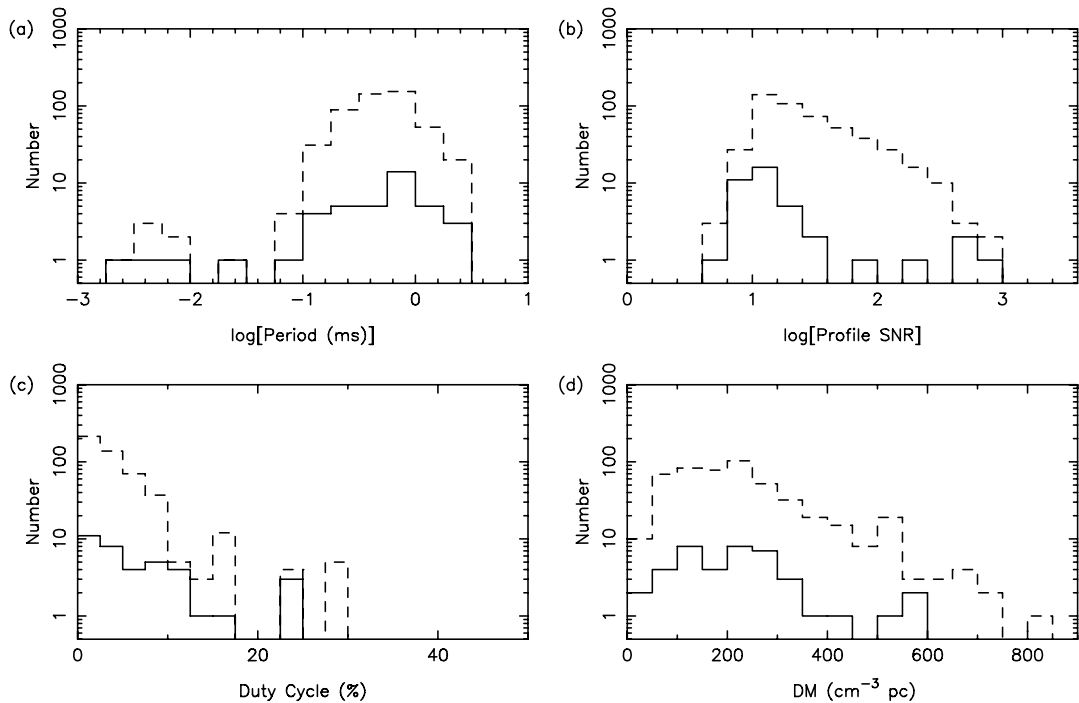


Figure 7. Histograms showing the distributions of (a) spin period, (b) pulse profile S/N, (c) pulse duty cycle and (d) DM values of all the pulsars in the test sample (dashed lines) and pulsars missed by the ANN (solid lines).

6 SUMMARY AND DISCUSSION

ANNs have been developed to aid searches for radio pulsars in a data base of ~ 16 million pulsar candidates generated from a recent re-analysis of the PMPS. The ANNs were trained using small sets of characteristic scores derived from the pulsar candidate plots generated for human inspection. Around 92 per cent of the pulsars present in a test sample of ~ 2.5 million pulsar candidates can be recovered by our ANNs.

It is likely that pulsars from the test sample were missed due to one of three reasons: poor training of the ANNs on MSPs, abnormal candidate plots generated by our search software or unbalanced training sets. Future implementations should avoid unbalanced training sets or bias the training sets towards the objects of interest. A larger number of false positives from the ANN are beneficial for searches of the inherently rare objects in the data set, namely pulsars (e.g. Belokurov et al. 2003).

To test if the ‘contamination’ from non-pulsars in the results set could be further reduced, the threshold for pulsar identification, z_1 , was increased to 0.7, 0.8 and 0.9. In each case, the numbers of genuine pulsar to non-pulsar candidates recovered by the ANN were 1:24, 1:23 and 1:20, respectively; however, the corresponding recovered fractions of pulsars were 89, 86 and 81 per cent. In a search for pulsars, these few per cent could be potential new discoveries. As such, higher thresholds should only be used when the number of candidates produced by the ANN is unmanageable. Improving the detection efficiency of our ANNs will be the subject of future work. Improvements in this area are likely to depend upon better representation of the two-dimensional diagnostic plots in our input vectors. These planes are particularly useful for discriminating against narrow-band and impulsive RFI.

ANNs are only capable of classifying the inputs given to them based on the training received. By training the ANN using a set of pulsars with particular characteristics, we reduce the possibility of

uncovering atypical, unusual or unexpected phenomena. Therefore, it is important to use training sets of pulsars with a wide variety of properties and displaying phenomena such as scintillation, scattering, intermittency and binary motion. As described in Section 4.4, MSPs display somewhat different candidate plots to their standard pulsar counterparts. Separate ANN training using only data from MSPs may be required to find these pulsars. For more exotic pulsars, such as relativistic binary pulsars, any training sample will be limited in size. To find these systems, it might be possible to form training sets from simulated pulsar signals covering a wide range of pulsar and binary parameters. However, it is expected that ANNs trained with simulated training sets will not perform as well as those based on real data due to the subtle effects of instrumentation and RFI environments. In new pulsar surveys where the search data may vary from those of previous surveys, for example in the number of frequency channels and the sampling time, dedicated observations of known pulsars will be required to build a training data base of MSPs and the standard population of pulsars.

A complementary class of ANNs are unsupervised ANNs which require no desired or ‘target’ vector during training. The best example of such an ANN is the Kohonen Self-Organizing Map (SOM; e.g. Kohonen 2001). SOMs provide a way of representing multidimensional data in a lower number of dimensions, generally the two dimensions of a map. Similar input vectors share similar regions on these maps. Such an ANN could be used to divide the pulsar candidates into sub-classes such as MSPs, standard pulsars, noise signals and even common RFI signals. Although not optimal for candidate selection, such ANNs will be investigated in future work.

Future pulsar surveys will probe larger volumes of both real space and the parameter space associated with radio pulsars. The SKA will have a sensitivity that will allow the discovery of all 20 000–30 000 pulsars beaming towards Earth and visible from the shortlisted sites in South Africa and Western Australia. Inspecting the candidates from such surveys will be a tremendous data analysis task. For

illustration, scaling the PMPS up to an all-sky survey would result in an increase of approximately a factor of 40 in the number of pulsar candidates. Using the same search algorithm as in our recent re-analysis of the PMPS and assuming an inspection time of 1 s per pulsar candidate, viewing all the candidates from such a survey would take over 20 yr. This figure does not take into account beams that contribute many erroneous candidates due to RFI and that are relatively easy to flag and avoid using graphical selection tools. However, as we have already discussed, these cuts can increase the risk of missing genuine pulsars that lie near to RFI in phase space. Using an ANN and assuming the same recovered fraction of candidates of 0.5 per cent the total inspection time would come down to just over 1 month, vastly reducing the work load on human observers.

We would like to stress that simple ANNs, like those presented in this work, should not yet be treated as a complete replacement for human inspection of pulsar candidates. Humans are still best placed to spot anything unusual or interesting about the individual pulsar candidates being viewed. Because of the significant time saving, of around two orders of magnitude, ANNs might be best used for first passes over search output data before a more detailed manual inspection with graphical selection tools.

ACKNOWLEDGMENTS

This research was partly funded by grants from the Science & Technology Facilities Council. The Australia Telescope is funded by the Commonwealth of Australia for operation as a National Facility managed by the CSIRO. NM acknowledges the support of the Studienstiftung des deutschen Volkes and the ERASMUS exchange programme. We thank John Brooke and members of The University of Manchester School of Computer Science for useful discussions. We would like to thank Sir Francis Graham-Smith for useful discussions and manuscript reading. We also acknowledge Alessandra Forti and The University of Manchester Particle Physics group for use of the TIER2 computing facility³.

³ <http://www.hep.manchester.ac.uk/computing/tier2>

REFERENCES

- Belokurov V., Evans N. W., Du Y. L., 2003, MNRAS, 341, 1373
 Bishop C. M., 1995, Neural Networks for Pattern Recognition. Oxford Univ. Press, Oxford
 Cordes J. M., Kramer M., Lazio T. J. W., Stappers B. W., Backer D. C., Johnston S., 2004, New Astron. Rev., 48, 1413
 Eatough R. P., 2009, PhD thesis, Univ. Manchester
 Eatough R. P., Keane E. F., Lyne A. G., 2009, MNRAS, 395, 410
 Faulkner A. J. et al., 2004, MNRAS, 355, 147
 Firth A. E., Lahav O., Somerville R. S., 2003, MNRAS, 339, 1195
 Hewish A., Bell S. J., Pilkington J. D. H., Scott P. F., Collins R. A., 1968, Nat, 217, 709
 Jenet F., Miller A., Rodriguez-Zermeno A., Stovall K., van Straten W., 2007, BAAS, 38, 735
 Keith M. J., Eatough R. P., Lyne A. G., Kramer M., Possenti A., Camilo F., Manchester R. N., 2009, MNRAS, 395, 837
 Kohonen T., 2001, Self-organizing Maps. Springer, Berlin
 Lintott C. J. et al., 2008, MNRAS, 389, 1179
 Lorimer D. R., Kramer M., 2005, Handbook of Pulsar Astronomy. Cambridge Univ. Press, Cambridge
 Manchester R. N. et al., 2001, MNRAS, 328, 17
 Smits R., Kramer M., Stappers B., Lorimer D. R., Cordes J., Faulkner A., 2009a, A&A, 493, 1161
 Smits R., Lorimer D. R., Kramer M., Manchester R., Stappers B., Jin C. J., Nan R. D., Li D., 2009b, A&A, 505, 919
 Storrie-Lombardi M. C., Lahav O., Sodre L. Jr., Storrie-Lombardi L. J., 1992, MNRAS, 259, 8P
 van Leeuwen J., Stappers B. W., 2010, A&A, 509, A7
 Westphal A. J. et al., 2005, in Mackwell S., Stansbery E., eds, Lunar and Planetary Institute Science Conference Abstracts Vol. 36, 36th Annual Lunar and Planetary Science Conference. p. 1908
 Zhang Y., Li L., Zhao Y., 2009, MNRAS, 392, 233

This paper has been typeset from a TeX/LaTeX file prepared by the author.